REPORT DOCUMENTATION PAGE

AFRL-SR-BL-TR-00-

0012

1. AGENCY USE ONLY *(Leave blank)*	2. REPORT DATE	3. REPORT TYPE AND DATES COVERED
	November 1999	FINAL TECHNICAL REPORT 1 Mar 98-30 Nov 98

4. TITLE AND SUBTITLE
STURCTURE PROPERTY RELATIONSHIPS IN TI3 SI C2

5. FUNDING NUMBERS
F49620-98-1-0314

61102F
2306/BS

6. AUTHOR(S)
M. W. BARWOUM

7. PERFORMING ORGANIZATION NAME(S) AND ADDRESS(ES)
DREXEL UNIVERSITY
DEPARTMENT OF MATERIALS ENGINEERING
PHILADELPHIA PA 19104

8. PERFORMING ORGANIZATION REPORT NUMBER

9. SPONSORING/MONITORING AGENCY NAME(S) AND ADDRESS(ES)
AIR FORCE OFFICE OF SCIENTIFIC RESEARCH
110 DUNCAN AVENUE SUITE B115
BOLLING AFB DC 20332-8050

10. SPONSORING/MONITORING AGENCY REPORT NUMBER

11. SUPPLEMENTARY NOTES

12a. DISTRIBUTION AVAILABILITY STATEMENT
APPROVED FOR PUBLIC RELEASE, DISTRIBUTION IS UNLIMITED

12b. DISTRIBUTION CODE

13. ABSTRACT *(Maximum 200 words)*

The dislocation structure of a typical low angle boundary associated with a kink band in a sample of Ti 3 sIc 2 deformed at room temperature was studied by HRTEM. the boundary had both tilt nd twist components. To account for both, the boundary was interpreted to be composed of parallel, alternating, mixed perfect dislocations with two different Burger's vectors lying in the basal plane at an angle of 120 o relative to one another. The boundary twist was provided by having an excess of one type of dislocation. The bitherto unreported structure of a low-angle boundary is attributed to the fact that all dislocations are confined to the basal planes.

20000118 064

14. SUBJECT TERMS	15. NUMBER OF PAGES
	22
	16. PRICE CODE

17. SECURITY CLASSIFICATION OF REPORT	18. SECURITY CLASSIFICATION OF THIS PAGE	19. SECURITY CLASSIFICATION OF ABSTRACT	20. LIMITATION OF ABSTRACT
U	U	U	

Final Report

Structure Property Relationships in Ti_3SiC_2

By

M. W. Barsoum

Department of Materials Engineering

Drexel University, Philadelphia PA 19104

Proposal Number

F49620-98-1-0314

Contract Monitor
Dr. Alexander Pechenik
U.S. Air Force, AFOSR-NC
Bolling AFB,
110 Duncan Ave., Wash. DC
703 696 7236

Introduction:

In December 11, 1997 we were awarded a $25 K, contract for nine months starting Jan. 1, 1998. During this period we carried out some fundamental work on the deformation mechanism of Ti_3SiC_2 at the transmission and high-resolution transmission electron microscopic level. Two refereed publications resulted from this work [1,2]. Our main findings are described below.

i) The dislocation structure of a typical low angle boundary associated with a kink band in a sample of Ti_3SiC_2 deformed at room temperature was studied by HRTEM [1]. The boundary had both tilt and twist components. To account for both, the boundary was interpreted to be composed of parallel, alternating, mixed perfect dislocations with two different Burger's vectors lying in the basal plane at an angle of 120° relative to one another. The boundary twist was provided by having an excess of one type of dislocation. This hitherto unreported structure of a low-angle boundary is attributed to the fact that all dislocations are confined to the basal planes. This paper was published in Philosophical Magazine Letters in 1999, a copy of which is attached.

ii) TEM of aligned macro-grained samples of Ti_3SiC_2, deformed at room temperature, shows that the deformed microstructure is characterized by a high density of perfect basal plane dislocations with Burgers vector $1/3\langle 11\bar{2}0\rangle$. The dislocations are overwhelmingly arranged either in arrays, wherein the dislocations exist on identical slip planes, or in dislocations walls, wherein the same dislocations form a low angle grain boundary normal to the basal planes. The arrays propagate across entire grains and are responsible for deformation by shear. The walls form as a result of the formation of kink bands. A dislocation-based model, that builds on earlier ideas proposed for kink band formation in hexagonal metallic single crystals, is presented that explains most of the microstructural features. The basic elements of the model are: shear deformation by dislocation arrays, cavitation, creation of dislocation walls and kink boundaries, buckling and delamination. The delaminations are not random, but successively bisect the delaminating sections. The delaminations and associated damage are contained by the kink boundaries. This containment of damage is believed to play a major role in endowing Ti_3SiC_2, and by extension related ternary carbides and nitrides, with their damage tolerant properties. This dislocation-based model that goes a long way in explaining the mechanical response of Ti_3SiC_2especially in compression. This paper was published in Metallurgical and Materials Transactions in July 1999. A reprint of the paper is attached to this final report.

References:

1) L. Farber, I. Levin and M. W. Barsoum, "HRTEM Study of a Low-Angle Boundary in Plastically Deformed Ti_3SiC_2", Phil. Mag. Letters., **79**, 163 (1999).

2) M. W. Barsoum, L. Farber and T. El-Raghy, "Dislocations, Kink Banks and Room Temperature Plasticity of Ti_3SiC_2", Met. Mat. Trans., **30A,** 1727-1738 (1999).

PHILOSOPHICAL MAGAZINE LETTERS, 1999, VOL. 79, NO. 4, 163–170

High-resolution transmission electron microscopy study of a low-angle boundary in plastically deformed Ti_3SiC_2

L. FARBER†, I. LEVIN‡ and M. W. BARSOUM†

† Department of Materials Engineering, Drexel University, Philadelphia, Pennsylvania 19104, USA
‡ Ceramics Division, National Institute of Standards and Technology, Gaithersburg, Maryland 20899, USA

[*Received 15 September 1998 and accepted 23 December 1998*]

ABSTRACT

The dislocation structure of a typical low-angle boundary associated with a kink band in a sample of Ti_3SiC_2 deformed at room temperature was studied by high-resolution transmission electron microscopy. The boundary had both tilt and twist components. To account for both, the boundary was interpreted to be composed of parallel alternating mixed perfect dislocations with two different Burgers vectors lying in the basal plane at an angle of 120° relative to one another. The boundary twist was provided by having an excess of one type of dislocation. This hitherto unreported structure of a low-angle boundary is attributed to the fact that all dislocations are confined to the basal planes.

§ 1. INTRODUCTION

Recently we have shown that large-grained oriented polycrystalline samples of (hexagonal) Ti_3SiC_2 loaded in compression at room temperature deformed plastically, by a combination of delamination of individual grains, shear and kink band formation (Barsoum and El-Raghy 1998). Transmission electron microscopy of the undeformed and deformed samples revealed that the vast majority of dislocations were perfect, of $\mathbf{b} = \frac{1}{3}\langle 11\bar{2}0\rangle$ type, lying in the basal planes (Farber *et al.* 1998). Furthermore, these basal plane dislocations were mobile and multiplied as a result of the room-temperature deformation. All the stacking faults observed also lay in the basal planes. Since the basal interatomic vector in Ti_3SiC_2 is by far the shortest full translation vector in this structure, no other perfect dislocations are likely and none is observed.

The formation of kink bands in crystalline solids is a rather uncommon mode of deformation. It was first proposed by Orowan (1942) to account for the sudden and peculiar kinks observed upon the deformation of single-crystal wires of zinc or cadmium loaded parallel to their basal or slip planes. In ceramics, kink bands have been reported for SiC single-crystals compressed parallel to their basal or slip planes at 1500°C (Suematsu, *et al.* 1991).

Hess and Barrett (1949) proposed a dislocation-based model to explain kink band formation, wherein the kink boundaries are formed by the generation of pairs of edge dislocations of opposite signs that move in opposite directions. To form kink bands, the dislocation pairs must form on many parallel, regularly spaced

Philosophical Magazine Letters ISSN 0950-0839 print/ISSN 1362-3036 online
http://www.tandf.co.uk/JNLS/phl.htm
http://www.taylorandfrancis.com/JNLS/phl.htm

slip planes, a small number of atomic spacings apart. They also noted that kinking should be more prevalent in hexagonal metals and alloys having an axial c/a ratio greater than 1.732; otherwise the material could accommodate the stress by twinning. The c/a ratio in Ti_3SiC_2 is 5.76 and it is thus not surprising that it is susceptible to kinking. Later, Frank and Stroh (1952) detailed how a thin elliptical kink could nucleate and grow, almost perpendicular to the basal planes, by the generation of dislocation pairs at the tip of the kink, when the applied shear stress exceeded some critical value. Both models assumed the kink boundaries to be composed of edge dislocations.

Because it is only recently that Ti_3SiC_2 has been available in dense pure bulk form (Barsoum and El-Raghy 1996), little is known about the atomistics of its deformation mechanisms. The goal of this contribution is to analyse by high-resolution transmission electron microscopy (HRTEM) the dislocation structure of a low-angle kink boundary, formed as a result of plastic deformation.

§ 2. Experimental details

This work was carried out on large-grained oriented samples of Ti_3SiC_2 that were deformed in compression at room temperature. Details of the synthesis and processing of the specimens can be found elsewhere (Barsoum and El-Raghy 1998). The final microstructure is one in which oriented macrograins (1–4 mm in length with aspect ratios of 20–40) are arranged in a chevron pattern. Specimens with dimensions 2 mm × 2 mm × 4 mm were deformed at room temperature by compression in an Instron testing machine at a strain rate of $2.5 \times 10^{-1}\,s^{-1}$.

The specimens for the HRTEM study were prepared by conventional polishing and dimpling, followed by ion thinning in a Gatan precision ion-polishing system. A JEOL 3010-UHR microscope, with point-to-point resolution of 1.7 Å and information limit of about 1.4 Å operated at 300 keV, was used for structural imaging. The phase-contrast analysis was made in terms of geometrical distortions only, without any attempt to interpret the contrast in terms of atomistic structure. The images were recorded with a Gatan charge-coupled device camera and analysed using commercial Gatan software. The diffraction contrast experiments were performed on a Phillips EM-430 microscope operated at 200 keV.

§ 3. Results and discussion

A bright-field image of the area containing a typical kink band is shown in figure 1 (*a*). The band, indicated by the arrows, is aligned parallel to the beam direction. A HRTEM image of the same boundary is shown in figure 1 (*b*). The fast Fourier transform of the same image filtered in the $11\bar{2}0$-type reflections is shown in figure 1 (*c*). This figure clearly shows that the boundary is composed of dislocations which in this $[1\bar{1}00]$ projection appear as edge dislocations with a Burgers vector $b_{obs} = d_{11\bar{2}0} = 1.54$ Å. The mean distance y between dislocations in the boundary is about 6.2 Å, from which the tilt angle $\omega \approx 15^\circ$ is easily calculable. Segments of the crystal on both sides of the boundary are oriented with their $\langle 1\bar{1}00 \rangle$ zone axes approximately parallel to the beam direction. The misorientation between the two parts of the crystal can be described by a combination of a tilt $\phi = 15^\circ$ about the $\langle 1\bar{1}00 \rangle$ direction and a twist $\psi = 2^\circ$ normal to the boundary which is parallel to the $\langle 11\bar{2}0 \rangle$ direction (figure 2 (*a*)).

Interestingly enough, and as shown in figure 2 (*b*), the $\mathbf{b}_{obs}$ value of 1.54 Å does *not* correspond to either perfect ($\mathbf{b}_1$, $\mathbf{b}_2$ and $\mathbf{b}_3$) or partial ($\mathbf{b}_{p1}$, $\mathbf{b}_{p2}$ and $\mathbf{b}_{p3}$) Burgers

(*a*)

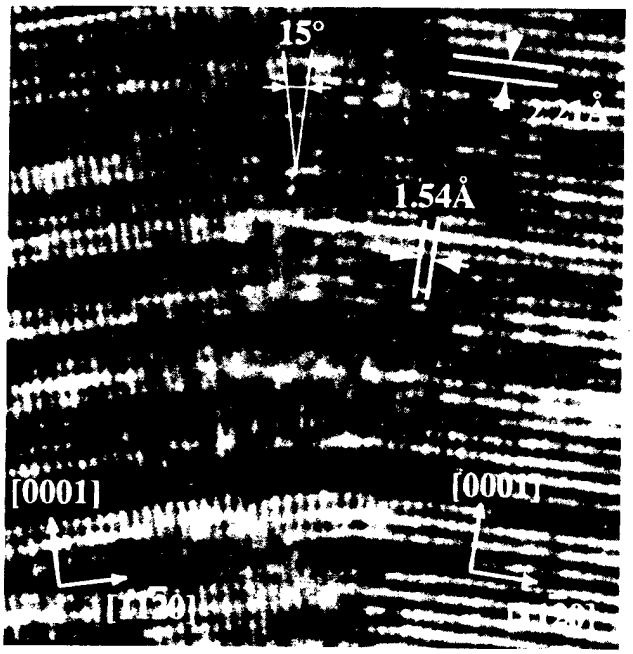

(*b*)

Figure 1. (*a*) Bright-field image of the area containing a kink band. (*b*) Structural image of the part of the boundary indicated by arrows in (*a*). The boundary plane is oriented parallel to the electron beam direction. (*c*) The same structural image filtered in $11\bar{2}0$-type reflections using fast Fourier transform. An example of the Burgers circuit drawn around one of the dislocations is shown by the rectangle; the termination of the extra plane is indicated by the arrow. The locations of all other dislocations are designated by the symbol $\perp$.

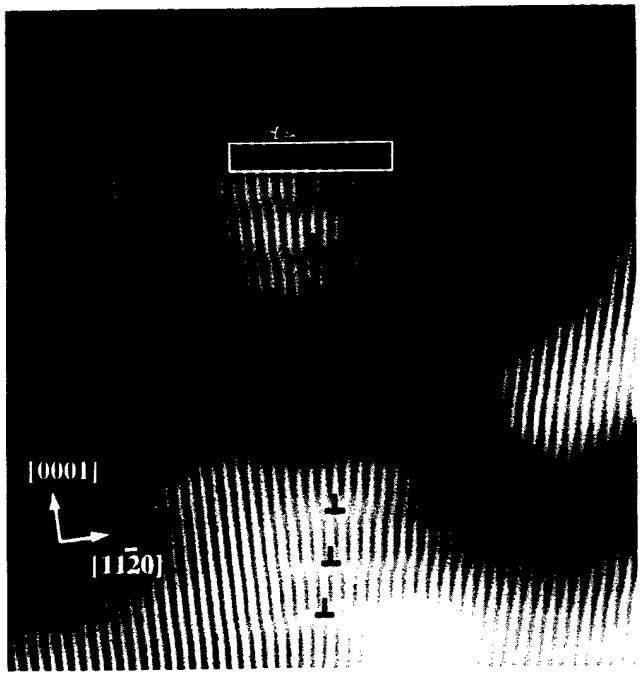

1 (*c*)

vectors in Ti_3SiC_2. Consequently, $\mathbf{b}_{obs}$ must be a projection on to the $\langle 11\bar{2}0\rangle$ direction of either perfect ($\mathbf{b}_2$ or $\mathbf{b}_3$) or partial ($\mathbf{b}_{p2}$ or $\mathbf{b}_{p3}$) dislocations. However, if $\mathbf{b}_{obs}$ were a projection of a partial, it should be bound by a basal-plane stacking fault. However, neither phase nor diffraction contrast revealed any stacking faults. Thus, $\mathbf{b}_{obs}$ must be a projection of perfect mixed dislocations $\mathbf{b}_2$ or $\mathbf{b}_3$, with an angle $\Theta = 30^\circ$ between its Burgers vector and the dislocation line (figure 2 (*b*)).

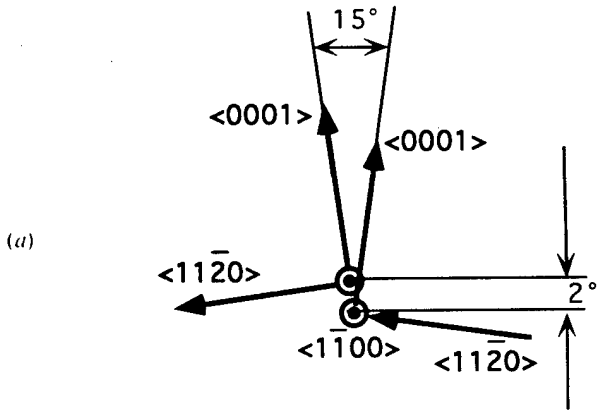

(*a*)

Figure 2. (*a*) Schematic representation of the misorientation between two parts of the crystal on both sides of the boundary. (*b*) Schematic representation of the [0001] projection showing the dislocation line, and projections of observed and possible Burgers vectors.

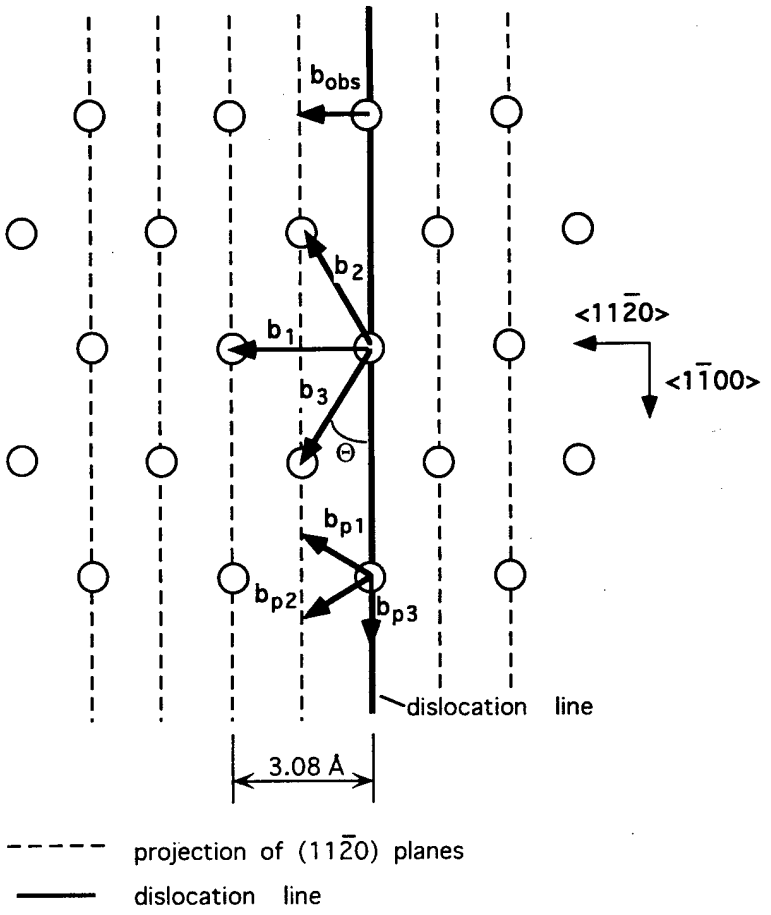

2(*b*)

Based on the foregoing discussion, both the image and the misorientation between the two parts of the crystal can be explained if we assume that the boundary is composed of alternating parallel mixed dislocations with Burgers vectors $\mathbf{b}_2$ and $\mathbf{b}_3$. We propose that, in such a configuration, the edge components of the dislocations provide the tilt, whereas the twist is accommodated by the difference in number of these mixed dislocations (figure 3(*c*)).

To estimate the stability of the walls composed of mixed dislocations with $\Theta = 30^\circ$, consider the elastic forces acting on the dislocations. The Burgers vector of a mixed dislocation can be expressed as the vector sum of the edge and screw components:

$$\mathbf{b} = \mathbf{b}_e + \mathbf{b}_s. \tag{1}$$

where $\mathbf{b}_e$ is normal to, and $\mathbf{b}_s$ is parallel to, the dislocation line. Since the basal plane is the only slip plane in this structure, the force F_x which acts on a mixed dislocation in the basal plane in a direction normal to the dislocation line can be calculated. For two parallel dislocations, this force is the sum of the force $E_{x\,\mathrm{edge}}$ between their edge components and the force $F_{x\,\mathrm{screw}}$ between their screw components

$$F_x = F_{x\,\mathrm{edge}} + F_{x\,\mathrm{screw}}. \tag{2}$$

The absolute values of these forces are given by

$$|F_{x\,\mathrm{edge}}| = \frac{\mu(b\sin\Theta)^2}{2\pi(1-\nu)}\,\frac{x(x^2-y^2)}{(x^2+y^2)^2}. \tag{3a}$$

$$|F_{x\,\mathrm{screw}}| = \frac{\mu(b\cos\Theta)^2}{2\pi}\,\frac{x}{x^2+y^2}. \tag{3b}$$

where y is the distance between the two slip planes containing the dislocations, x is the distance measured along the slip direction, μ is the shear modulus and ν is Poisson's ratio (Cottrell 1953). For the screw components, the force is attractive, when they have opposite signs. For the edge components, the force is attractive when they have the same sign provided that $x < y$.

According to figure 1(*c*), the edge components of all the dislocations have the same sign. Thus, $F_{x\,\mathrm{edge}}$ is always attractive for $x < y$. The sign of the screw components, on the other hand, cannot be determined from the experimental results. They can be envisaged, however, as arranged in one of two limiting configurations: the screw components of all the dislocations have the same sign (figure 3(*a*)), or neighbouring dislocations have screw components of opposite sign (figure 3(*b*)). The stability of each of these two configurations is considered below.

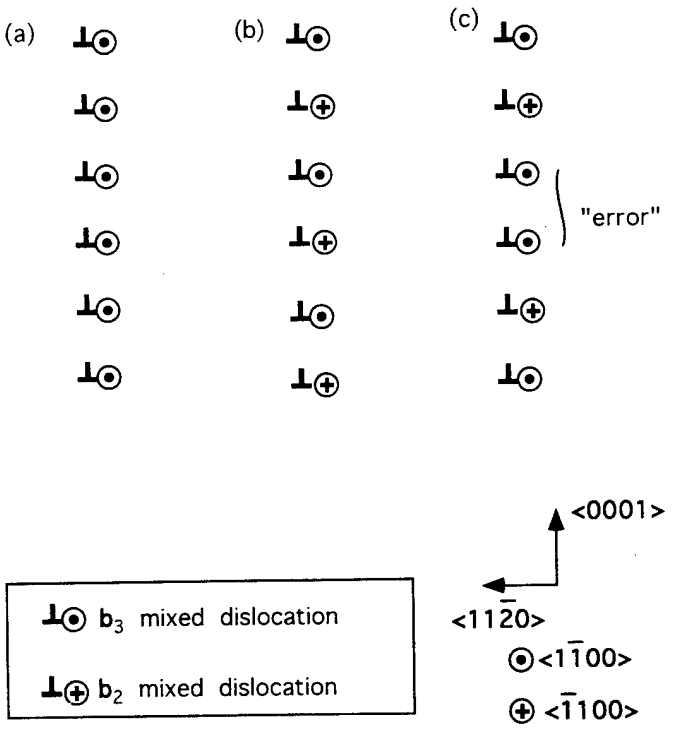

Figure 3. Possible arrangements of mixed dislocations $\mathbf{b}_2$ and $\mathbf{b}_3$ in a dislocation wall: (*a*) screw components are in the same direction; (*b*) alternating screw components; (*c*) same as (*b*), but showing a stacking error in the screw component. Configuration (*a*) is unstable, whereas (*b*) and (*c*) are stable.

According to equation (3*a*) and (3*b*), for two parallel dislocations with $\Theta = 30^\circ$ lying in different basal planes, the following inequality is valid for any x and y:

$$|F_{x\,\mathrm{edge}}| < |F_{x\,\mathrm{screw}}|, \tag{4}$$

that is interaction between the screw components is stronger than that between the edge components. Thus, if the screw components of two parallel mixed dislocations with $\Theta = 30^\circ$ have the same sign, repulsion will prevail and the configuration shown in figure 3(*a*) is unstable. Conversely, when the screw components of neighbouring dislocations alternate (figure 3(*b*)), the configuration is stable.

The configuration shown in figure 3(*b*), however, *cannot* account for the 2° twist observed since the numbers of each type of dislocations are equal. It is only by having an excess of dislocations of either type that the twist can be accounted for. The twist angle ω is given by

$$\omega = \frac{b_s}{y_s}, \tag{5}$$

where y_s is the average distance between the excess dislocations of one sign. The relative number N of the excess dislocations can be evaluated as follows:

$$N = \frac{y_s}{y} = \frac{\mathbf{b}_s}{\mathbf{b}_e}\frac{\phi}{\omega}. \tag{6}$$

From the experimental data, substituting $\mathbf{b}_s = \mathbf{b}\cos 30^\circ$, $\mathbf{b}_e = \mathbf{b}\sin 30^\circ$, $\phi = 15^\circ$ and $\omega = 2^\circ$, one obtains $N \approx 13$. In other words, an error in the $\mathbf{b}_2/\mathbf{b}_3$ sequence occurs, on average, once every 13 dislocations. As noted above, for large N, the wall is stable. As N goes to unity (i.e. figure 3(*a*)), the wall becomes unstable. At some intermediate N, the wall becomes critically stable. Using equations (2), (3*a*) and (3*b*), the force on the excess dislocations in a wall can be calculated. For example, it can be shown that any wall with $N \geqslant 6$ (figure 3(*c*)) is stable. This implies that the experimentally determined twist, for which $N \approx 13$, is also a stable configuration.

Several attempts to prove directly the presence of the alternating sequence of mixed dislocations in the wall by diffraction-contrast analysis in a conventional transmission electron microscope were unsuccessful; separate dislocations within the wall could not be resolved, obviously owing to the small mean interdislocation distance (0.62 nm).

Generally, in metals, twist is usually accommodated by the formation of a crossed grid of screw dislocations. Such an arrangement, however, is not possible for the boundary considered since the vast majority of dislocations in Ti_3SiC_2 are perfect and lie in the basal plane (Farber *et al.* 1998).

Acknowledgements

The deformed specimens for this study were provided by Dr T. El-Raghy (Drexel University); his cooperation and help are greatly appreciated. This work was sponsored by the US Air Force Office of Scientific Research. Partial support by the Stein Foundation is greatly appreciated by L. F.

References

Barsoum, M. W., and El-Raghy, T., 1996, *J. Am. Ceram. Soc.*, **79**, 1953; 1998, *Metall. Trans.* (to be published).

Cottrell, A. H., 1953, *Dislocations and Plastic Flow in Crystals* (Oxford University Press).

Farber, L., Barsoum, M. W., Zavaliangos, A., El-Raghy, R., and Levin, I., 1998, *J. Am. Ceram. Soc.*, **8**, 1677.

Frank, F. C., and Stroh, A. N., 1952, *Proc. phys. Soc.* B, **65**, 811.

Hess, J. B., and Barrett, C. S., 1949, *Trans. AIME*, **185**, 599.

Orowan, E., 1942, *Nature*, **149**, 643.

Suematsu, H., Suzuku, T., Iseki, T., and Mori, T, 1991, *J. Am. Ceram. Soc.*, **74**, 173.

Dislocations, Kink Bands, and Room-Temperature Plasticity of Ti_3SiC_2

M.W. BARSOUM, L. FARBER, and T. El-RAGHY

Transmission electron microscopy (TEM) of aligned, macrograined samples of Ti_3SiC_2, deformed at room temperature, shows that the deformed microstructure is characterized by a high density of perfect basal-plane dislocations with a Burgers vector of $1/3\langle 11\bar{2}\ 0\rangle$. The dislocations are overwhelmingly arranged either in arrays, wherein the dislocations exist on identical slip planes, or in dislocations walls, wherein the same dislocations form a low-angle grain boundary normal to the basal planes. The arrays propagate across entire grains and are responsible for deformation by shear. The walls form as a result of the formation of kink bands. A dislocation-based model, that builds on earlier ideas proposed for kink-band formation in hexagonal metallic single crystals, is presented, which explains most of the microstructural features. The basic elements of the model are shear deformation by dislocation arrays, cavitation, creation of dislocation walls and kink boundaries, buckling, and delamination. The delaminations are not random, but successively bisect the delaminating sections. The delaminations and associated damage are contained by the kink boundaries. This containment of damage is believed to play a major role in endowing Ti_3SiC_2 and, by extension, related ternary carbides and nitrides with their damage-tolerant properties.

I. INTRODUCTION

RECENTLY, we reported on the fabrication and characterization of the ternary compound Ti_3SiC_2.[1–5] This compound is a layered hexagonal material in which almost close-packed planes of Ti are separated from each other by hexagonal nets of Si; every fourth layer is a Si layer. The C atoms occupy the octahedral sites between the Ti layers. This compound combines an unusual set of properties. Like metals, it is a good electric and thermal conductor, readily machinable, relatively soft (with a Vickers hardness of 4 GPa), and highly thermal-shock resistant. Above 1200 °C, the material deforms in a pseudoplastic manner, with significant ductility. At 1300 °C, its "yield" stresses in flexure and compression are 100 and 500 MPa, respectively. Like ceramics, it is elastically rigid, oxidation resistant,[3] and stable to at least 1700 °C in inert atmospheres and in vacuum.[2]

Basal-plane dislocation arrays of limited extent are observed in undeformed Ti_3SiC_2 samples.[6] However, room-temperature deformation significantly increases their extent, indicating that dislocations multiply and are mobile at room temperature. The arrays are composed of perfect basal-plane dislocations with a Burgers vector of $1/3\ \langle 11\bar{2}\ 0\rangle$. A key characteristic of the Ti_3SiC_2 structure, the appreciation of which is important in understanding the atomistics of its mechanical properties, is that the basal interatomic vector is by far the shortest full translation vector in this structure. Thus, nonbasal dislocations are very unlikely, and, indeed, none are observed.

Oriented coarse-grained (1 to 3 mm) polycrystalline samples of Ti_3SiC_2, loaded in compression at room temperature, deform plastically.[5] When the basal planes are oriented favorably to the applied stress, substantial (>20 pct) deformation occurs by shearing along those planes. When the basal planes are parallel to the applied load, deformation occurs by a combination of delamination of individual grains and the formation of shear and kink bands. The buckling and kink-band formation initiates at the corners of the cubic samples.[5]

Kink-band formation has been invoked to explain the deformation of numerous materials and structures such as highly constrained rocks,[7] organic crystals,[8] card decks,[9] rubber laminates,[10] oriented polymer fibers,[11–15] wood,[16] graphite fibers,[17,18] and laminated C-C and C-epoxy composites,[19,20,21] among others. The formation of kink bands in crystalline solids, however, is an uncommon deformation mechanism. As first reported by Orowan,[22] kink-band formation is a deformation mode typically observed in hexagonal metals such as zinc and cadmium. Typically, single-crystal rods with the *c*-axis almost parallel to the rod axis undergo local collapse under compression to form a kink. Kinking is predicted in hexagonal metals and alloys having an axial *c/a* ratio greater than 1.732; *i.e.*, in metals wherein twinning is unlikely.[23] With a *c/a* ratio of 5.76, it is not surprising that Ti_3SiC_2 is susceptible to kinking. This mode of deformation was also observed in hexagonal boron nitride[24] and SiC single crystals deformed at temperatures (>1500 °C) above which the dislocations are mobile.[25]

Orowan proposed that kink bands develop by a special mechanism in which glide lamellae of uniform thickness snap abruptly to a tilted position. He concluded that kink boundaries consist of planes which bisect the angle between the glide planes on either side of them, and along which the dislocations are concentrated.[22] Later, Hess and Barrett[23] proposed a model to explain the formation of these kink bands by the regular glide of dislocations. The major elements of this model are summarized schematically in Figures 1(a) through (c). Initially, and upon loading, elastic bending (Figure 1(a)) creates a maximum shear stress at two sections of the column (Figure 1(b)). Above a critical value, this

M.W. BARSOUM, Professor, L. FARBER, Postdoctoral Fellow, and T. EL-RAGHY, Research Assistant Professor, are with the Department of Materials Engineering, Drexel University, Philadelphia, PA 19104.

Manuscript submitted November 3, 1998.

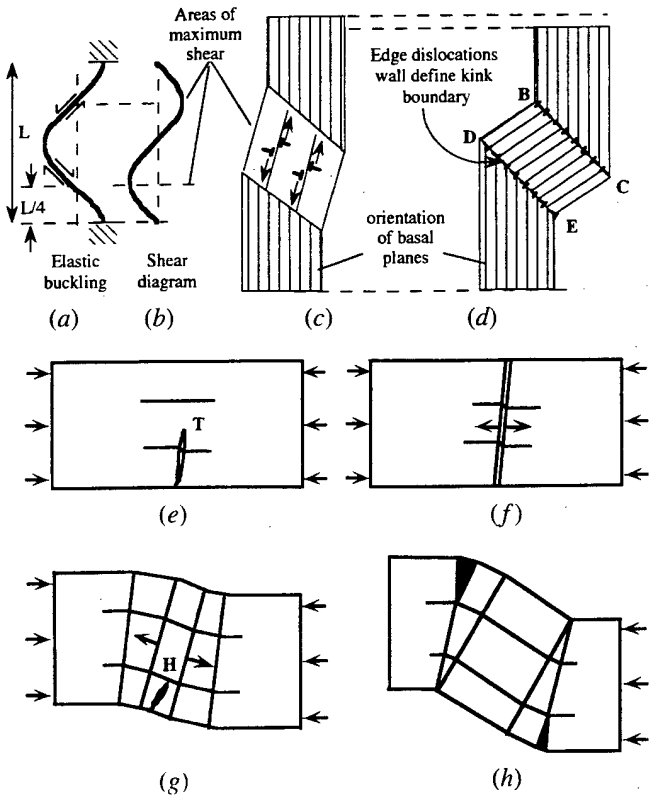

Fig. 1—Scheme of kink-band formation (*a*) through (*d*) from Ref. 23 and (*e*) through (*h*) from Ref. 26: (*a*) elastic buckling, (*b*) corresponding shear diagram, and (*c*) initiation of pairs of dislocations in areas of maximum shear. (*d*) Kink band and kink boundaries comprised of edge dislocations of one sign giving rise to the classic stove-pipe shape. (*e*) Initiation of kink band at tip of narrow kink, *T*. (*f*) Intersection of *T* with free surface, removes the attractive energy between the walls and allows them to separate and move in opposite directions. (*g*) and (*h*) Repetition of same process to create more dislocation walls.

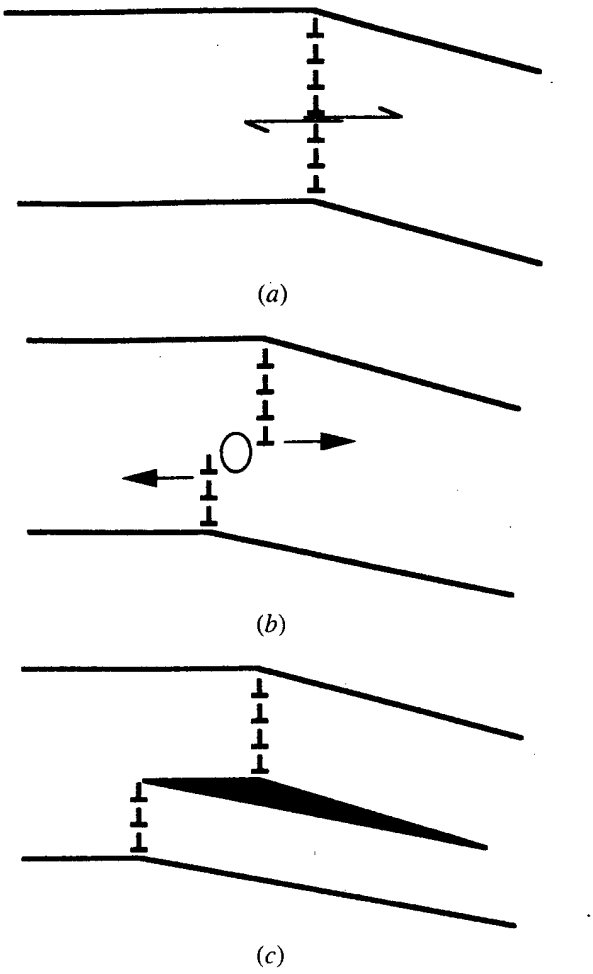

Fig. 2—(*a*) through (*c*) Nucleation of a crack normal to a dislocation wall when the latter is subjected to a shear stress.[27]

shear stress is sufficient to create, within the volume that is to become the band, pairs of dislocations of opposite sign that move in opposite directions (Figure 1(c)). The end result is two regions of severe lattice curvature, separated from each other and from the unkinked crystal by well-defined kink planes (BC and DE in Figure 1(d)). These kink planes or boundaries have an excess of edge dislocations of one sign, which, in turn, are responsible for the lattice rotations observed.[23]

And, whereas Hess and Barrett did not elaborate on the specific mechanism for the formation of the dislocations walls, Frank and Stroh did.[26] In their model, pairs of dislocations of opposite sign nucleate and grow at the tip of a thin elliptical kink (labeled T in Figure 1(e)) when the applied shear stress exceeds some critical value. As long as the pair of dislocation walls are within the crystal or grain, they are attracted to each other, but are held apart by the external stress (Figure 1(e)). The strong attraction disappears, however, when the walls extend to the free surface, at which point the dislocation walls become parallel planes (Figure 1(f)). The minimum value of lattice rotation that will allow the dislocation wall to grow *via* the mechanism they propose is about 3 deg for metals. A continuing stress should then force the walls apart. The process of wall formation can then be repeated at the same source, resulting in the generation of new dislocation walls (Figures 1(g) and (h)). If the component dislocations in successive walls are not on the same slip plane, the walls could unite or collapse, forming a kink plane or boundary. The collapse does not occur simultaneously along the whole wall but sequentially, starting at one end of the kink boundary and moving to the other end, as shown schematically in Figure 1(h).

The formation of kink boundaries is, thus, explained by the accumulation of several walls in a relatively thin region. Hess and Barrett also suggested that the first wall can be stopped by some defect, resulting in an accumulation of walls near this defect. Alternatively, as proposed by Frank and Stroh, since each wall has a different angle to the external load, as a result of successive changes of lattice direction (Figure 1 (h)), the increase in the shear stress for each successive wall formed may result in their moving faster, leading to their accumulation.

The dislocation wall extending across a grain is a low-energy configuration (Figure 2(a)). However, if, for some reason, the dislocation wall is forced to divide (Figure 2(b)), Stroh[27] has shown that the magnitude of the stress between the ends can be high enough to open a crack of limited length propagating normal to the wall, as shown in Figure 2(c). Such cracks were observed in kinked regions of SiC single crystals deformed at high temperature[25] and in h-BN.[24]

At present, the atomistic details of the deformation mechanisms that are operative in Ti_3SiC_2 are unknown. The goal of this work is to shed some light on these mechanisms by carrying out a transmission electron microscopy (TEM) characterization of the line-defects structure present in room-temperature–deformed samples of Ti_3SiC_2.

II. EXPERIMENTAL PROCEDURE

The fabrication procedure for the material has been described in detail elsewhere.[5] In short, titanium (99.99 pct, −325 mesh, supplied by Alta Group, (Arvada, CO)), SiC (99.7 pct, d_m = 4 μm, supplied by Performance Ceramics (Peninsula, OH)), and C powders (99 pct, d_m = 1 μm, supplied by Aldrich (Milwaukee, WI)) were weighed and dry mixed in a V-blender (Patterson–Kelly Co. (East Stroudsburg, PA)) for 2 hours to yield the Ti_3SiC_2 stoichiometry. Oriented coarse-grained (2 to 3 mm) polycrystalline samples were fabricated *via* a hot forging operation in a channel die, followed by a 1600 °C, 24-hour anneal, during which the grains, which were oriented during the forging operation, grew significantly.[5]

Small cubes were machined and deformed under compression at room temperature as a function of orientation. The details on the mechanical testing are given in Reference 5. For this work, a specimen was deformed at a strain rate of 0.05 s^{-1} in the direction for which the basal planes of most grains were at angle of 25 deg to the loading direction. Clear, unambiguous evidence for the formation of a thin deformation shear band, parallel to the basal planes, was observed by optical microscopy. For TEM characterization of the deformed material, sections were taken so that the plane of the TEM sample was normal to the basal plane and contained the load axes.

Thin foils for TEM were prepared by slicing 200-mm-thick sections, followed by thinning and polishing by the Gatan Dimple Grinder (Model 656) and ion milling at 5 kV/20 mA by the Gatan Precision Ion Polishing System (Model 691). Microstructural observation was performed using a JEOL* 100CX2 transmission electron microscope operated at 100 kV.

*JEOL is a trademark of Japan Electron Optics Ltd., Tokyo.

III. RESULTS

Scanning electron microscopy (SEM) of the deformed material showed that, in agreement with previous work,[5] the deformation is confined to narrow bands containing kink bands, cracks, and delaminated grains. Some lamellas within individual grains were buckled. The TEM observations also show that the dislocation density in the deformed material is significantly higher than that in the undeformed material, in agreement with previous work.[6] Tilting and contrast analysis confirm that all dislocations are basal, with Burgers vectors of $\mathbf{b} = 1/3\ \langle 11\bar{2}\ 0\rangle$.

The dislocations can be categorized, according to their association with other dislocations, as belonging to either arrays that are parallel to, or dislocations walls that are normal to, the basal planes. Single dislocations are scarce. A kink boundary is defined here as a narrow (typically <50 nm) region between two misoriented regions of a single grain. It is assumed to contain multiple walls that are either closely spaced or have collapsed. Each type of arrangement is described subsequently in more detail.

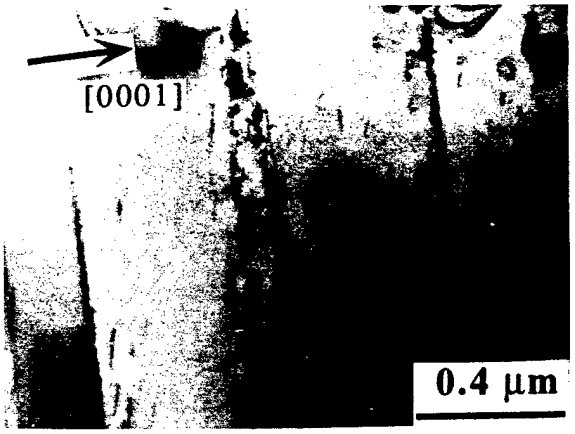

Fig. 3—Bright-field image of an area containing dislocation arrays. The specimen is close to the orientation where basal planes are in an edge-on position

A. *Basal-Plane Arrays (Figure 3)*

This arrangement, wherein the dislocations all lie in the same basal slip plane, is the most common feature found in various regions of the deformed specimen and can be seen in most of the micrographs shown herein. Typical examples are shown in Figure 3. In agreement with previous results,[6] most of the arrays propagate through the whole transparent field of view and, thus, presumably propagate across the entire grain. Within an array, the dislocations are parallel and more or less equidistant. Tilting of the grains so that the basal planes are in an edge-on position shows that the dislocations within an array propagate on the *identical* slip plane.

Some arrays are more "dense" than others. In many grains, the dense arrays are spaced more or less equidistantly, with several less-dense arrays interspersed between them, as shown in Figure 3. The distances between the dislocations within an array range from 20 to 200 nm. The distances between dense arrays typically range from 100 to 500 nm. The denser arrays with smaller interdislocation distances are usually spaced more closely. In several cases, two closely spaced dense arrays are observed at a position where a single dense array could be expected. The dislocation density in regions containing arrays, such as that shown in Figure 3, is about 10^{10} cm^{-2}. Contrast analysis reveals that the arrays are composed of identical, perfect mixed basal dislocations.

B. *Dislocation Walls*

In this arrangement, the dislocations are parallel and positioned in different basal planes, one under another, so that the whole arrangement is normal to the basal planes and constitutes a low-angle boundary (Figure 4(a)). Contrast analysis (Figures 4(b) and (c)) reveals that the wall is composed of edge and mixed dislocations.

As clearly documented in Figures 6 through 8, the vast majority of dislocation walls are observed within kink bands and bent regions, as well as at the tips of most, if not all,

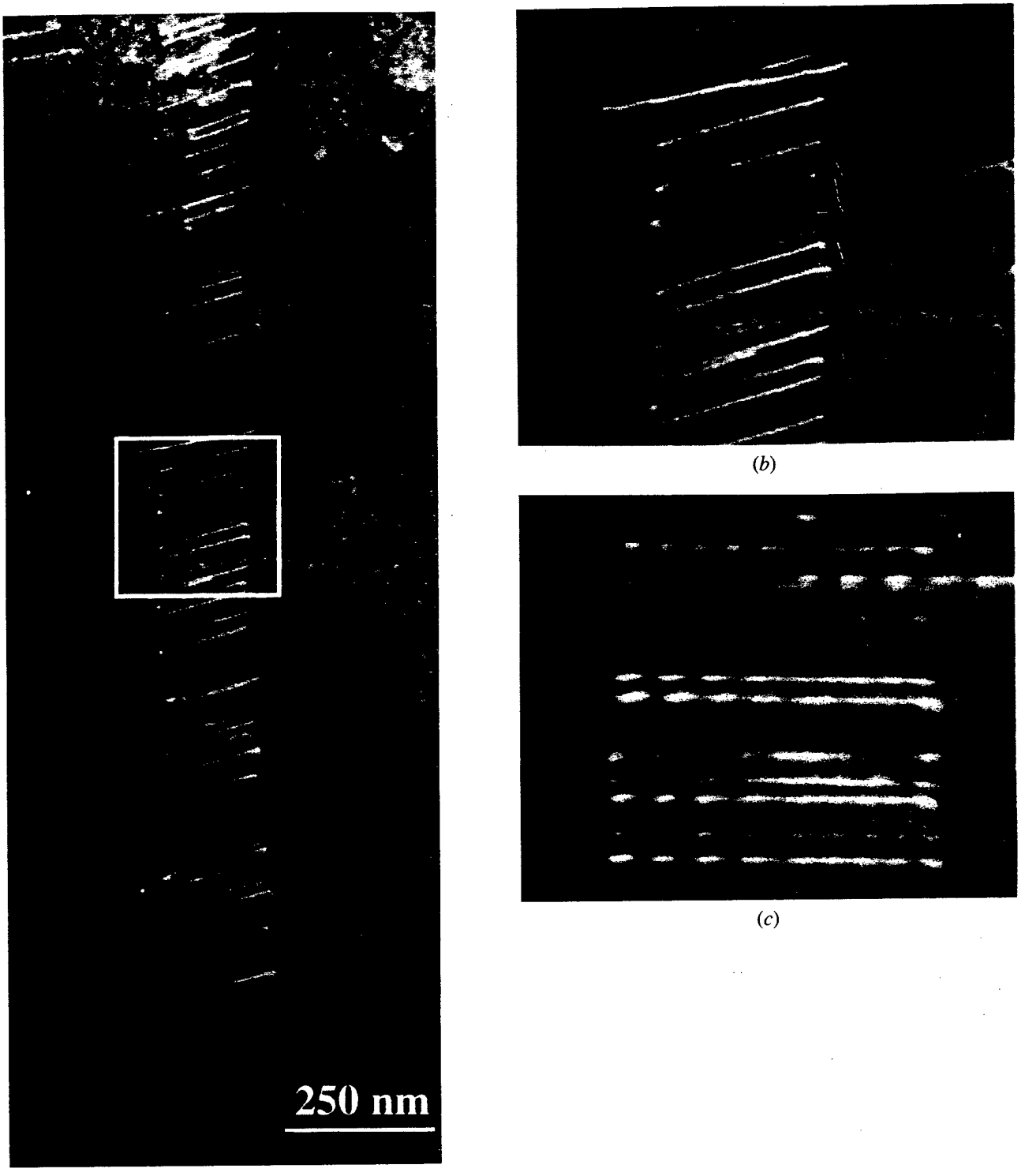

Fig. 4—(*a*) Dislocation wall; dislocations are parallel and positioned in different basal planes one under another. (*b*) Same area as white square in (a), but at higher magnification (imaged in g $\langle 33\bar{6}\ 0\rangle$). (*c*) Weak beam image of the same area as in (b), but tilted and imaged in g of $\langle 3\bar{3}\ 00\rangle$. Dislocations that become invisible in (c) are perfect edge dislocation; those that remain visible are mixed dislocations.

delamination cracks. Furthermore, all the walls observed in this work are found to terminate at either free surfaces or dislocation arrays. Typically, the interdislocation distances within the walls do not exceed 15 nm.

An example of a collection of dislocation walls which constitute a kink boundary is shown in Figure 5. The misorientation provided by this kink boundary between two parts of a crystal is a combination of an ≈14-deg tilt around the $\langle 1\bar{1}\ 00\rangle$ direction and an ≈1.6-deg twist around the $\langle 11\bar{2}\ 0\rangle$ direction, *i.e.*, around the direction normal to the boundary.

Fig. 5—Bright-field image of a kink boundary showing that it is composed of dislocation walls (indicated by arrows).

Within the walls, indicated by arrows in Figure 5, the dislocations are well resolved. The separation between the walls decreases toward the center of the curvature (*i.e.*, to the left), so that, at some point, the walls practically converge (not shown). Imaging in 0008-type reflections has shown that the walls within the boundary provide a sequential lattice misorientation.

Fully separated walls are usually observed in bent, delaminated regions of the specimen. A typical example is shown in Figure 6(a), which shows a bent region that is delaminated in three slices (designated as S_1 through S_3) and contains dislocation walls and arrays. A selected-area diffraction (SAD) of the region where the basal planes are close to the edge-on position and where the transmitted beam is close to a $\langle 1\bar{1}\ 00\rangle$ direction is shown in Figure 6(b). The SAD demonstrates that there is a lattice rotation around the $\langle 1\bar{1}\ 00\rangle$ axes, *i.e.*, normal to the plane of Figure 6(b). Dark-tilt imaging with 0008 reflections shows that the rotation is sequential and is provided by the walls: each section is bound by two dislocation walls and is tilted at some small (2 to 4 deg) angle to neighboring domains. In addition to the tilt around the $\langle 1\bar{1}\ 00\rangle$-type direction, the walls provide a sequential twist around the $\langle 11\bar{2}\ 0\rangle$ direction.

A schematic of the same area is shown in Figure 6(c). The dislocation walls (designated by the letter W) propagate normal to the basal planes across each slice. Arrays (designated by the letter A) propagate along the basal planes, through the bend, and into the adjacent matrix regions (this is not very clear in Figure 6(a), but is clearly seen in the TEM upon tilting). Tilting does not reveal other dislocations. The walls are well separated and spaced more or less equidistantly. The interdislocation distance within the walls is considerably smaller than that in the arrays.

C. *Kink Bands*

A typical example of a region containing two closely spaced, oppositely oriented kink bands is shown in Figure 7(a), for which a schematic, where the projection of the basal planes are reproduced, is shown in Figure 7(b). In each kink band, the lattice is misoriented relative to neighboring areas. The changes in lattice orientation occur mostly at the kink boundaries. Typically, the misorientation provided by these kink boundaries can be described by a combination of a tilt around the $\langle 1\bar{1}\ 00\rangle$ direction and a twist around the direction normal to the boundary, which is parallel to the $\langle 11\bar{2}\ 0\rangle$ direction. The basal planes are close to the edge-on orientation, and the ones containing dislocation arrays are seen as fine lines in Figure 7(a). Generally, the tilt across kink bands observed in this study varied from $\approx$12 to 60 deg, while the twist varied from $\approx$0.5 to 12 deg. Figure 7(a) shows two kink bands near the edges of the tilt spectrum; the top kink band is tilted by $\approx$15 deg and the bottom by $\approx$47 deg (Figure 7(b)). Typically, separate dislocation walls are only resolvable within the kink boundaries when the misorientation is small ($<$12 to 17 deg.)

Two types of cracks associated with the kink bands are observed: delamination and cracks along kink boundaries. By far the more important and prevalent are the delamination cracks. These cracks are *always* associated with kink bands. The delamination cracks also occur along the basal planes *near or at dense* dislocation arrays.

The delamination cracks are triangular in shape, with the obtuse angles at the kink boundaries and the acute angles propagating into the material on both sides of the boundary. The sizes and asymmetries of the delamination cracks varied (Figure 8). The larger cracks are typically asymmetric, with the longer part typically propagating into the kink band. Some of these cracks propagate across the entire kink band, *i.e.*, from kink boundary to kink boundary. The ends of the delamination cracks are typically bound at one side by the original kink boundary, which is dislodged parallel to the basal planes and outward relative to the kink bands. The other side propagates into the kink band and is typically bound by a single dislocation wall (Figures 8(a) and (d)).

Another example of delamination associated with kink boundaries is shown in Figure 8(b). In this figure, the kink boundary provides a misorientation of $\approx$16 deg and is composed of several dislocation walls (not resolved at the magnification shown, but well resolved at higher magnification). The overall shape of the crack and accompanying kink band is in good agreement with the scheme shown in Figures 2(c), *i.e.*, the kink boundary terminates at the obtuse angle and continues from one of the acute angles. The right end of the delamination crack shown in Figure 8(b) is bound by a single dislocation wall (not visible in this micrograph).

Yet another example of a delamination crack is shown in Figure 8(c). Here, a sliver of the material (denoted by S) adjacent to the obtuse angle of the crack near the kink boundary is delaminated and buckles in a direction opposite to that of the initial kink boundary (L).

In addition to the aforementioned delamination cracks, other much less frequently observed cracks that run along a kink boundary (denoted by the letter R in Figure 8(d)) are observed. These cracks are only observed at boundaries where the misorientation is high, typically, more than 50 deg. These cracks propagate at the obtuse angle of the

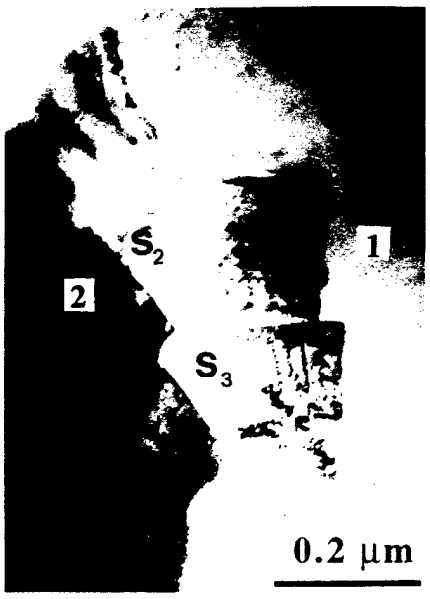

(a)

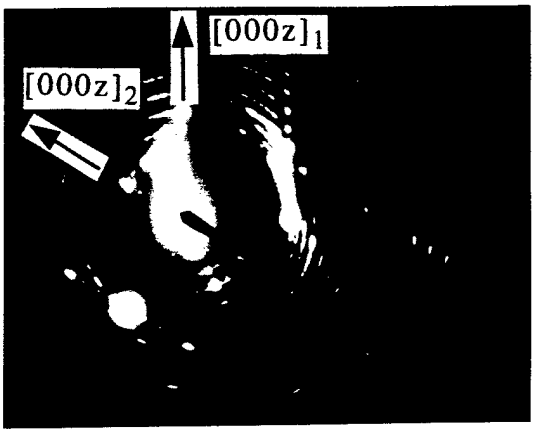

(b)

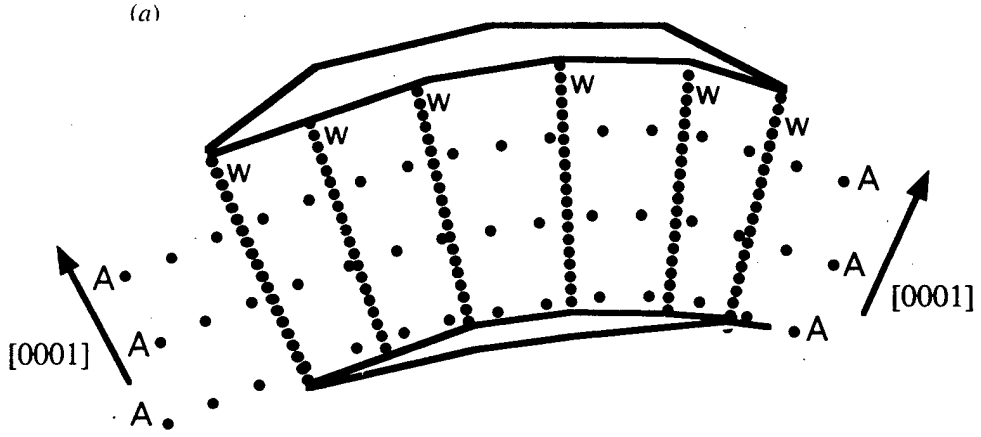

(c)

Fig. 6—(*a*) Bright-field image of a bent region delaminated in three slices S_1 through S_3 and containing separated walls and arrays. (*b*) Selected area diffraction from the same region, but tilted to an edge-on position for the basal planes demonstrating lattice rotation around $\langle 1\bar{1}\,00\rangle$ directions. (*c*) Schematic of S_2 showing walls (W) and arrays (A).

delamination cracks described previously and run parallel to the kink boundary.

IV. PROPOSED MODEL

Based on the foregoing results, we propose the following sequence of events to explain most of our experimental observations. The evidence is discussed in detail in the next section V. Consider the two adjacent grains, labeled S and P in Figure 9(a), subjected to a vertical load. The basal planes in grain S are aligned such that the resolved shear stress in the basal planes is nonzero. The basal planes in grain P, on the other hand, are parallel to the applied load. In this figure, the solid-gray area of width *W* is the section of grain P that buckles.

A. *Arrays and Shear Deformation*

When the resolved shear stress exceeds the critical value in grain S, it will deform by shear toward the lower left in Figure 9(a). This shear will be accommodated by the formation of dislocation arrays. The critical resolved shear stress in Ti_3SiC_2 at room temperature is estimated to be 36 MPa.[5] Grain P will not deform initially. The shear of grain S away from P, however, will create a cavity at the grain boundary between the two grains, as shown schematically in Figure 9(b).

B. *Cavitation and the Initiation of Buckling*

As a consequence of the formation of the cavity, the shaded volume will tend to relax, first elastically and then plastically, into that cavity. The plastic deformation is initially accommodated by the formation of dislocation arrays (parallel to the basal planes) that extend across the whole grain, as a direct result of the shear stresses between the shaded area and the remainder of the grain (Figure 9(b)). The change in shape can also be accommodated by the generation of dislocation walls normal to the applied load.

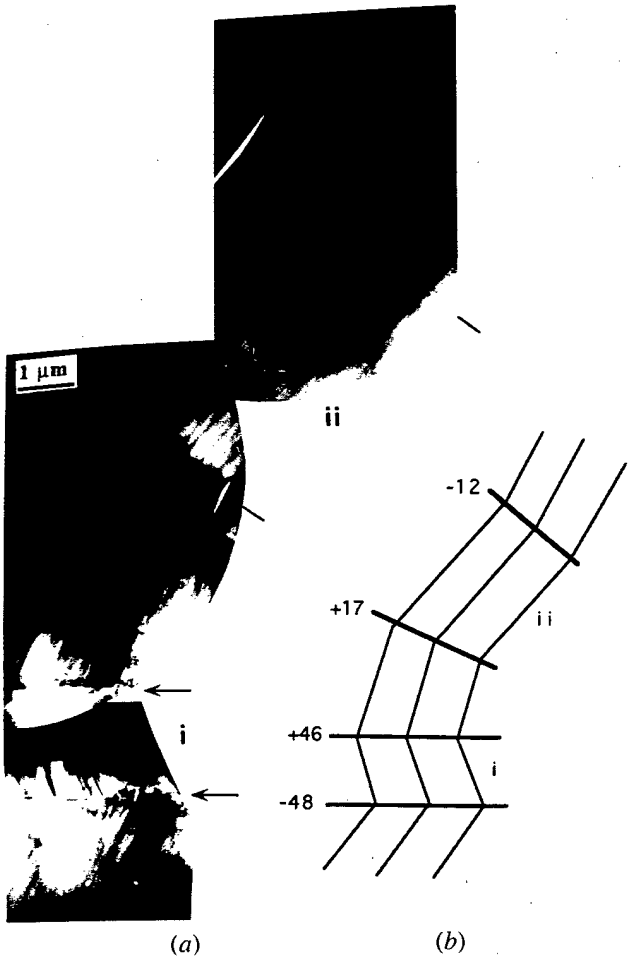

Fig. 7—(*a*) Bright-field image of and (*b*) schematic of a region containing two adjacent kink bands denoted as i and ii. The crystal is close to the edge-on position for the basal planes. The numbers show the measured rotation angles between the blocks of the crystal around $\langle 1\bar{1}\,00\rangle$ directions provided, mostly, by the kink boundaries.

These are depicted in Figure 9(b) as short horizontal lines within the shaded area.

C. *Kink-Band Formation*

Upon further loading, the shaded volume will, depending on its exact geometry relative to the location of the cavity and the local state of stress, plastically buckle into the void. Where along the length (L) of the lamella the shear is maximum depends on many factors, such as the length-to-width ratio of the buckling section, the location of the constraints relative to L, and the symmetry of the loading environment, among others.[23] For example, in Figure 1(a), the maximum shear is assumed to occur at $L/4$ and $3L/4$. Regardless of the exact locations of the areas of maximum shear, the formation of shear bands requires that dislocation pairs be emitted from the center of what is to become the kink band and move in opposite directions.[23] This is a fundamental distinction between deformation by shear and kink-band formation. For the sake of simplicity, the locations of maximum shear were chosen to be the areas labeled X and Y in Figure 9(b). It is the emission of dislocation walls of opposite sign from these locations that ultimately results in two kink bands, BC and DF, shown in Figure 9(c), or, equivalently, BC and DE, shown in Figure 1(d).

It is worth noting here that, as the lattice rotates as a result of the formation of the dislocation walls and kink boundaries, the maximum shear stresses increase, leading to an acceleration of the formation of these walls and, potentially, to local geometrical softening.[28]

Since the buckling and kinking occurs while maintaining the mechanical integrity of the grain,* then, perforce, the ends of the buckled volume (labeled A in Figure 9(c)) *must* shear toward the center of that grain. Here again, the shear occurs *via* dislocation arrays that form in the buckled region prior to the formation of the kink boundaries.

*As opposed to the total delamination, along the entire length of a uniaxially reinforced composite with weak interfaces loaded parallel to the lamella.

D. *Buckling and Delamination Cracks*

From a purely geometrical perspective (since only basal slip is available), the buckling or kink-band formation *cannot* occur in Ti_3SiC_2 without the formation of delamination cracks (Figures 9(c) and (d)). The thickness of the delaminated lamellae (*i.e.*, W) will depend on their radius of curvature (R), which, in turn, depends on the size of the cavity or void into which the material can buckle. The smaller the cavity, the higher the stresses needed to buckle and the thinner the lamella that are generated. Furthermore, thick lamellae form first; as the stress is increased, however, they sequentially delaminate at $W/2$, $W/4$, *etc.* One mechanism by which this can occur is shown in Figure 9(d). Upon further deformation, the two kink boundaries at locations C and D, in which the dislocations have the same sign, collapse into one, labeled G-H in Figure 9(d). Their delamination cracks merge and result in the larger delamination shown.

Since only a finite density of dislocations can be accommodated at any kink boundary before tensile stresses at the core of these dislocations exceed the rupture stress of the material, it is not surprising that delaminations initiate at these boundaries. This is shown in Figure 9(d), where, as a result of further bending, the original kink boundary splits into two roughly equal length shorter kink boundaries, labeled G and H. Energetically, the most probable and likely location for the initiation of the delamination cracks has to be at the intersection of an array and a kink boundary. This is why the central array (dotted line in region w in Figure 9(c)) is absent in Figure 9(d). Needless to say, the formation of a free surface at an array annihilates the defects in that array and eliminates the accompanying strain energy. Here again, shear of one lamella relative to the other has to occur *via* the dislocation arrays that are present in all lamellae. It is believed that a repetition of this mechanism results in thinner and thinner lamellae with sharper and sharper radii of curvatures.

E. *Damage Containment*

Not only are the delamination cracks intimately related to the formation of kink bands, but, as importantly, they are *contained* within these bands. Thus, for example, the small delamination cracks shown in Figure 9(d) are contained

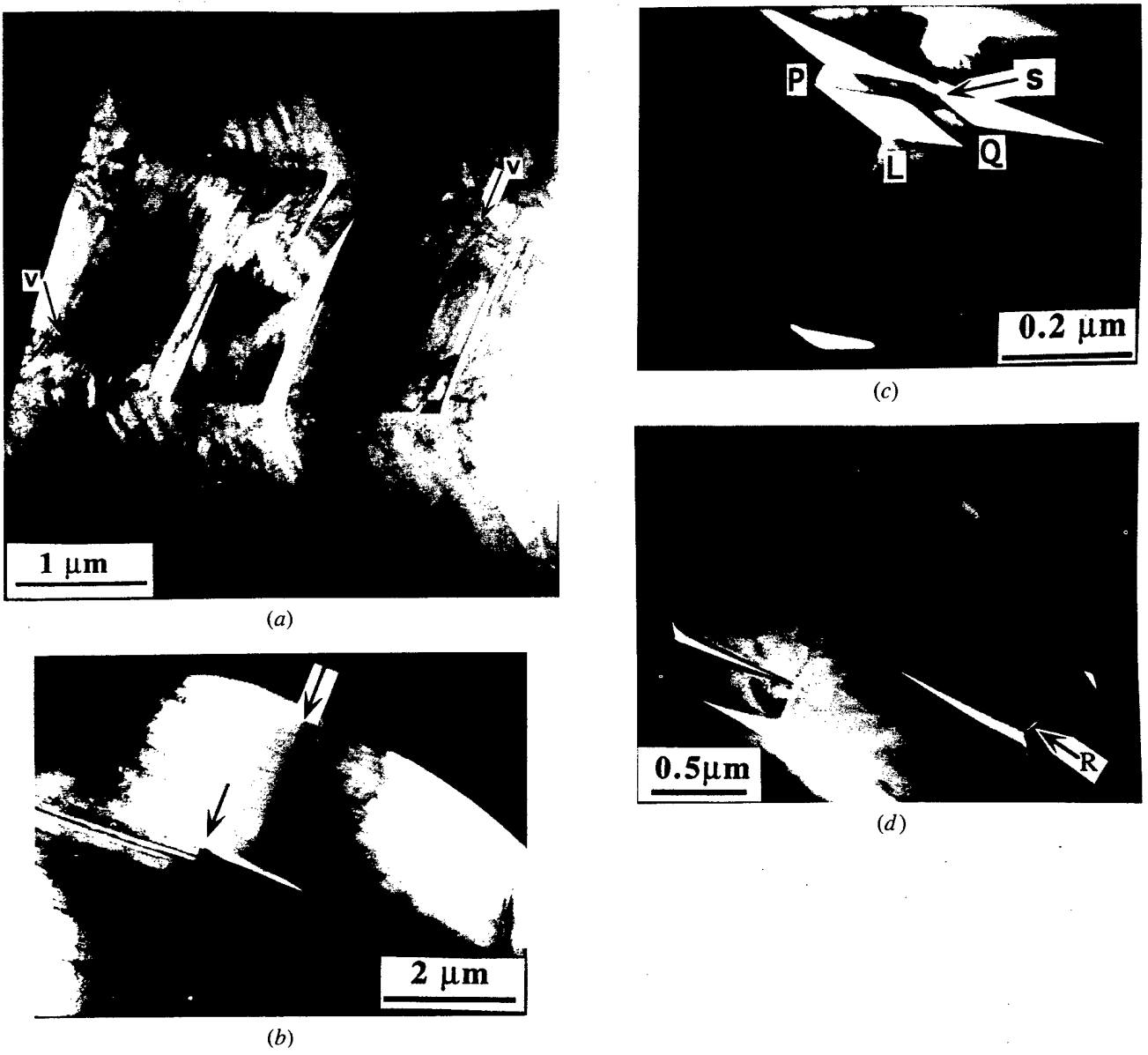

Fig. 8—(*a*) Bright-field image of a kink band with a high misorientation angle ("stove pipe") containing delamination cracks. Separate dislocation walls, which are generally normal to the basal planes, but are inclined to the kink boundaries, are denoted by V. (*b*) Delamination crack at a divided low-angle (≈16 deg) kink boundary shown by arrows. (*c*) Secondary delamination. Sliver S delaminates in cavity produced by delamination at kink boundary L forming obtuse angles P and Q. (*d*) Kink band containing crack along the kink boundary (denoted by R) in addition to delamination cracks.

between the kink boundaries B and F. This containment occurs regardless of how far the delamination cracks are from the edge of the specimen and, thus, cannot be attributed wholly to the reduction of the stress intensity at the crack tip due to changing geometry. The main reason is more fundamental: for the delaminations to extend beyond the kink bands requires that the kink boundary be moved ahead of the crack tip. This is energetically very costly and, thus, leads to a localized toughening of the material. As discussed subsequently, it this fundamental mechanism that is critical to endowing these layered carbides and nitrides with their damage-localization properties.

Finally, it should be pointed out that the model proposed here is just one of many possible scenarios. The local stress states are quite complicated, and the stochastic nature of where a kink band will form further complicates the problem. These qualifications notwithstanding, we believe that our model contains the fundamental elements of deformation under *compression* in these materials. These elements are shear deformation by arrays, cavitation, buckling, the formation of dislocation walls and kink boundaries, delaminations, and localization of damage.

V. DISCUSSION

Based on the foregoing results, there is little doubt that all deformation modes observed in Ti_3SiC_2 at room temperature, namely, shearing, kinking, buckling, and delamination, can be explained by the generation and conservative motion of perfect dislocations along the basal planes in either arrays or walls. This conclusion is in accord with our preliminary results, which did not reveal dislocation intersections (apart

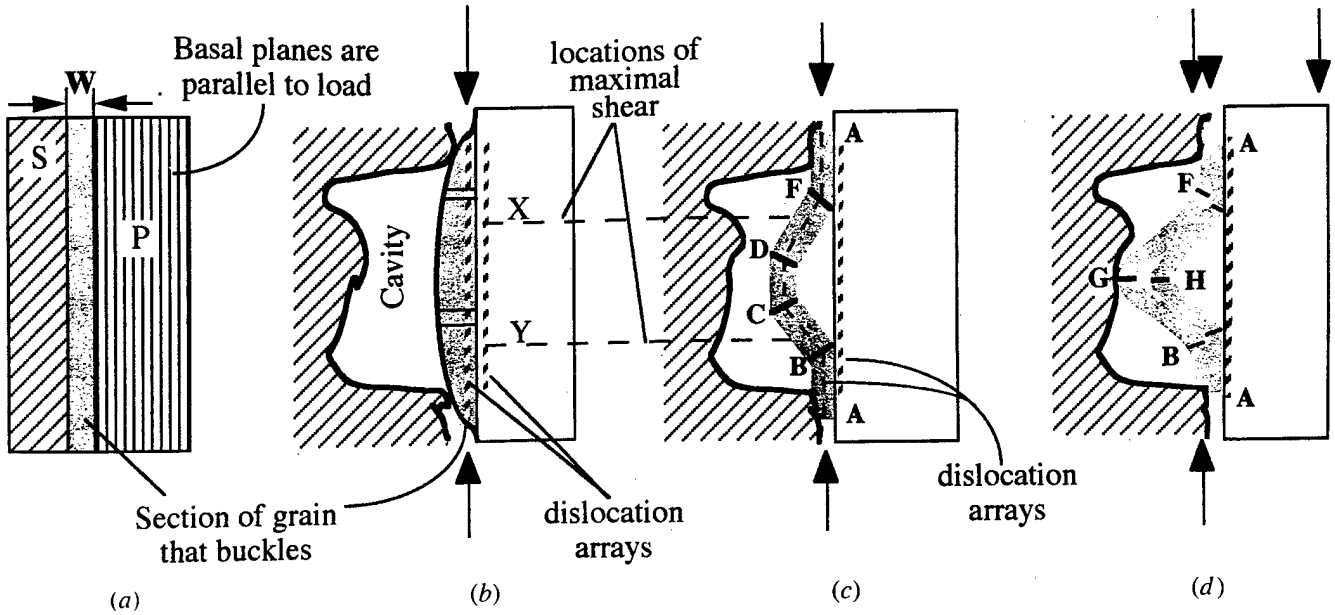

Fig. 9—Proposed model. (*a*) Initial state showing two grains S and P subjected to a vertical load. The gray area of width *W* is a portion of grain P that ultimately delaminates. (*b*) Initial deformation occurs by the formation of dislocation arrays (dashed vertical lines) and dislocation walls (short horizontal lines). Areas of maximum shear are assumed to be at X and Y. (*c*) The locations of maximum shear become the centers of two oppositely oriented kink bands BC and DF. (*d*) Further deformation forces the kink boundaries C and D to merge into the split into G and H. Note that even if the delamination cracks down the center of the gray area merge, they are still contained within the region bounded by B and F. Also note the disappearance of the dislocation array.

from the intersection of the arrays and dislocations walls discussed herein) or cross-slip. As noted in the Introduction, the absence of dislocations other than basal is not surprising, because of their much larger Burgers vectors.

In this section, evidence is presented for each element of our model. The following subsections correspond to those advanced in the previous section.

A. *Arrays and Deformation by Shear*

The arrays provide deformation by shear. In agreement with our previous results, the dislocation arrays propagate across the entire field of view of the transmission electron microscope and, thus, are presumed to propagate across the entire grain. (It is worth noting here that the grains in this material are quite large, ≈1 to 3 mm.) The uneven distribution of these dislocation arrays within the grains, together with the fact that the dislocations are arranged in arrays in the first place, strongly suggests that it is easier to move dislocations than to nucleate them. Their most likely source is, thus, the specimen surface or grain boundaries. The results also indicate that stacking faults and twins play a very small role, if any, in the deformation processes; none are observed.

The fact that the arrays propagate continuously through the kink bands and into the adjacent matrices (*e.g.*, Figures 6(a) and 7(a)) strongly suggests that they are formed first. Had they formed after the kink boundaries, they would have had to terminate at these boundaries. Even at the highest magnifications, the arrays appear continuous on either side of the kink boundaries.

B. *Cavitation*

Ti_3SiC_2 possesses less than five independent slip systems and it is, thus, not surprising that deformation results in the formation of numerous cavities and voids. Cavitation is observed in SEM for the deformed cubes used in this study. Such cavitation is also observed in polycrystalline samples deformed at temperatures greater than 1200 °C.[30]

C. *Kink-Band Formation*

Once cavitation occurs, thin lamellae of grains adjacent to the cavities will tend to relax into the latter. The relaxation is initially elastic, but is followed by two forms of plastic deformation. The first is the formation of dislocation arrays such as the ones shown in Figure 3 and depicted schematically in Figure 9(b). What characterizes these arrays is that they are not associated with dislocation walls or kink boundaries. However, based on the density of arrays observed, the misorientation they can impart is conservatively calculated to be ≈5 deg (Appendix A), a value significantly lower than that observed.

The second mechanism entails the generation of multiple dislocation walls from a given source. These types of dislocations are best exemplified by the dislocation walls shown in Figure 6. These micrographs are instructive in that they clearly show individual dislocation walls, the corresponding lattice rotation, and the presence of the arrays that allow these lamellae to shear with respect to each other. Furthermore, based on these micrographs, it is also not unreasonable to assume that these walls are produced sequentially from a single source. That is not always the case: for example, the two oppositely tilted kink bands shown in Figure 7 cannot be due to a single source.

According to Hess and Barrett,[23] a kink boundary forms by the collapse of a number of walls into a thin region. Figure 5 shows that indeed to be the case; at higher magnifications, the dislocation walls, constituting what appears to be a kink boundary at lower magnifications, are clearly

discernable. This is true only for low misorientations; at high misorientation angles, the details of the kink boundaries are not resolvable. Further evidence that the mechanism suggested by Hess and Barrett is operative is shown in Figures 7(a) and 8(a), where the classic stovepipe shape anticipated from the model (*e.g.*, Figure 1(c)) is clearly apparent.

One implication, not explicitly stated in the original models[23,26] but clearly shown in their schematics, is that V-shaped regions (shaded areas in Figure 1(h)) should form in the vicinity of the kink boundaries. Such features are quite common in Ti_3SiC_2. Typical examples are shown in Figure 8(a) and labeled with the letter V.

The exact mechanism for the formation of the dislocation walls is unknown at this time, but none of the evidence presented in this article refutes the Frank and Stroh model.[26] According to them, the minimum value of lattice rotation that will allow the dislocation wall to grow is about 3 deg for metals.[26] This value agrees well with the measured misorientation of the blocks separated by single dislocation walls in Figures 5 and 6. Also in agreement with the model, half-formed dislocation walls that terminate within the crystal (*e.g.*, the kink labeled H in Figure 1(g)) are not observed.

In their models, Hess and Barrett and Frank and Stroh assumed that the walls forming the kink boundaries are composed of pure edge dislocations, and the deviation from a pure tilt misorientation, experimentally observed in Zn single crystals, was ascribed to the presence of edge dislocations with two different Burgers vectors. However, no systematic study was carried out to confirm the previous hypothesis. Recently, we suggested that the misorientations provided by a dislocation wall in Ti_3SiC_2, namely, a combination of tilt around $\langle 1\bar{1}\ 00\rangle$ and twist around $\langle 11\bar{2}\ 0\rangle$, can only be explained if the wall was comprised of *mixed* dislocations.[29] The contrast analysis shown in Figure 4 supports this assumption, since it shows that, in addition to the pure edge dislocations that do disappear in $g = 3\bar{3}\ 00$, the wall contains dislocations that do not (compare Figures 4(b) and (c)). The latter must, therefore, be mixed dislocations. A complete analysis of the dislocation structure of a low-angle kink boundary observed in high-resolution TEM is given elsewhere.[29]

D. *Buckling and Delamination Cracks*

Once the local constraints around the grains relax, kinking and delaminations are possible. If for no other reasons than geometrical, the former is not possible without the latter.*

*This is only true for unconstrained deformations. Highly constrained rocks, for example, form a variety of kink bands without delaminations.[7]

The formation of any kink boundary of more than a few degrees must be accompanied by *delamination*.* The latter, in turn requires that the various lamellae shear relative to each other and relative to the unbuckled matrix (Figures 9(c) and (d)). This shear must be accommodated by the dislocation arrays.

*Delaminations of the type described in this work are not observed in metals; this phenomenon is unique to the layered ternary carbides and nitrides discussed here.

Hess and Barrett suggested, and our results indirectly confirm, that elastic buckling plays an important role in the formation of kink boundaries. The most compelling evidence for this hypothesis is the universal observation that, at all magnifications and for all lamellae, the ratio of their thickness to their radii of curvature is more or less a constant and of the same order of magnitude. In other words, delaminations occur when the elastic strains reach a certain threshold. For example, the lamellae that form at the corners of cubes compression loaded parallel to the basal planes in coarse grained–oriented samples are ≈10- to 40-μm thick; their corresponding radii of curvature are 40 to 60 μm.[5] Conversely, some of the lamellar thicknesses observed in this work are in the range from 0.2 to 4.3 μm; the corresponding radii of curvature are 0.5 to 15 μm.

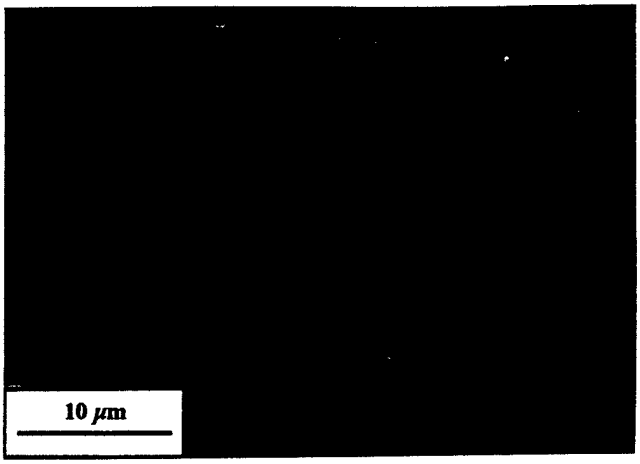

Fig. 10—SEM micrograph of nested and defoliated lamella. These features were created by scribing the sample surface with a sharp metal blade.

Further evidence for the importance of buckling is shown in Figure 7. The simplest explanation for the formation of the two oppositely oriented kink bands shown is that, at some time during the deformation process, the lamella was subjected to buckling stresses (*e.g.*, Figures 1(a) and (b)). Indeed, it is difficult to propose a model for the formation of the features shown in Figure 7, without invoking some sort of buckling mode.

Another important observation relates to the sequence by which the lamellae form. In any given region, where thick lamellae are present, thin ones are not observed, but not *vice versa*. In other words, the thick lamellae form first. With increasing stresses, the lamellae progressively split near their midpoints to form thinner lamellae, with sharper radii of curvature. This progressive delamination at *W*/2, *W*/4, *W*/8 *etc.*, is apparent in all the micrographs in which kink boundaries are observed. Two typical examples are shown in Figures 8(a) and (d), where the delamination cracks are not randomly distributed, but, rather, occur at specific locations, the most severe being at the midpoint of the thickness. It is only by invoking such a sequence of events that the constancy of the *W*/*R* ratio is most readily explainable.

The feature depicted schematically in Figure 9(d), where sharp lamellae appear to have defoliated from the bulk and are nested one in another, is one that has been observed many times in SEM micrographs of deformed samples. A typical example is shown in Figure 10. Based on the preceding discussion, we propose the following mechanism for their formation. As the segment BCDF (Figure 9(c)) is subjected to further loading, the kink boundaries C and D, in

which the dislocations have the same sign, merge to form the split boundary G-H (Figure 9(d)).

According to the elasticity theory, bending of laminates results in tensile stresses normal to the plane being bent. Since these stresses, which in this work are normal to the basal planes, are at a maximum midway through the thickness, *i.e.*, at *W*/2, it is not surprising that this plane is the first plane to delaminate.

The driving force for the nucleation of such cracks must be supplied by the large local elastic strains generated by the intersection of high misorientation kink boundaries and dense arrays. The primary evidence for this conjecture is the fact that the vast majority of delaminations occur near intersections of kink boundaries and dense dislocation arrays.

Figure 8(c) provides direct evidence that kink bands and delaminations form in areas of compressive stresses. The small kink band (S), shown in the center of Figure 8(c), buckles outward, as a result of compressive stresses. The buckling clearly occurs into a preexisting cavity that is formed as a result of the delamination of the larger kink band (L) that contains the smaller one. This micrograph is important for another reason. The two partial kink boundaries at P and Q (Figure 8(c)) have the same orientation as L. The easiest interpretation for how this may occur is to assume that the kink boundary splits in two, creating P and Q. If that were the only process occurring, however, the sum of the misorientation angles at P and Q should add up to that at L. From the micrograph, it is obvious that is not the case. Thus, one must assume that, in addition to splitting, some further kink-band formation was initiated upon forming S. The delamination cracks formed by this mechanism are by their very nature more symmetrical vis-à-vis the kink boundaries than the ones discussed in the next section.

E. *Damage Containment*

One of the more intriguing questions concerning the mechanical properties of Ti_3SiC_2 and related materials is their ability to contain damage under compression loading. At face value, this is a surprising result for a layered material that is so clearly prone to delamination and that lacks five independent slip systems. Based on the results of this study, the paradox can be partially resolved when it is appreciated that kink boundaries are extremely effective in containing the damage to the volume between them.

A perusal of the delamination cracks in Figures 7 and 8 quickly establishes that, with the exception of the types of delaminations discussed in the previous section (*i.e.*, the splitting of a boundary wall into two), the higher the misorientation across a kink boundary, the less these cracks extend outside the corresponding kink band. In other words, a correlation exists between the asymmetry of the delamination cracks and the degree of misorientation. For example, the delamination crack associated with the low-angle kink boundary shown in Figure 8(b) is about 1.8 μm and extends slightly more to the left than to the right (the main reason being that extension to the left entails a shift of the dislocation wall in that direction). Contrast analysis and tilting shows that the dislocation walls labeled by arrows in Figure 8(b) are two parts of the same kink boundary. Conversely, the two cracks associated with the high misorientation kink boundaries shown in Figure 8(d) are very asymmetric; they hardly extend outside the kink band shown, but appear to propagate readily toward the center of that band. The same is true in Figure 8(a). In both cases, the kink boundaries contain a higher density of dislocations and are, thus, more difficult to dislodge.

The overall spatial relationships between the delamination cracks and the dislocation walls shown in Figure 8(b) are almost identical to the ones proposed by Stroh[27] and shown schematically in Figure 2(c). Stroh showed that, if for some reason a dislocation wall is forced to divide as a result of a shear, the magnitude of the stress between the ends can be high enough to open a crack of limited length propagating normal to the wall. In other words, a mechanism exists for crack nucleation.

It thus appears that delamination cracks are created by, but then contained within, the kink boundaries. These dislocation walls or kink boundaries provide an intrinsic and local toughening mechanism, a mechanism that is unique to Ti_3SiC_2 and related ternaries. It means that, at some point during the delamination process, elastic energy is consumed on plastic deformation rather than on further opening of the crack. This conclusion is believed to be vital in endowing Ti_3SiC_2 with its damage localization properties.

As noted previously, cavitation is a necessary condition for deformation because it removes the constraints on the grains and allows for buckling and kink-band formation, thus promoting deformation. The stresses required to deform constrained samples are at least an order of magnitude higher than those of unconstrained samples. For example, the stresses at which aligned grains loaded parallel to the basal planes buckle is on the order of 200 to 300 MPa,[5] whereas the "yield" point under a Hertzian indentation—where the deformation is constrained by the surrounding matrix—is roughly an order of magnitude higher.[31]

Finally as in all materials, a competition exists between failure by shear or rupture. This balance appears to be biased toward rupture for randomly oriented polycrystalline samples of Ti_3SiC_2 loaded in compression or flexure at room temperature and is the main reason why the latter fail in a brittle manner.[5,30] At higher temperatures and/or for highly oriented microstructures at room temperature, the balance tips toward shear and kink-band formation. This conclusion would partially explain why the deformation mode of randomly oriented polycrystals above 1200 °C is quasi-plastic.[30]

VI. SUMMARY AND CONCLUSIONS

The TEM observations of room-temperature–deformed, macrograined samples of Ti_3SiC_2 conclusively show that the deformation of individual grains in Ti_3SiC_2 can be explained by the generation and conservative motion of perfect basal dislocations in either arrays or walls. The arrays are parallel to the basal planes and, for the most part, extend across entire grains and provide the mechanism by which the grains or parts of grains (*i.e.*, lamellae) shear relative to each other. Dislocation walls accommodate the buckling and kinking of lamellae that form parallel to the basal planes. The accumulation, and sometimes eventual collapse, of dislocation walls into a narrow region creates the kink boundaries. A dislocation-based model that builds on ideas first proposed by Hess and Barrett and Frank and Stroh is presented that explains many of the microstructural features observed at

the TEM and SEM levels. The basic elements of the model are shear deformation by dislocation arrays, cavitation, the creation of dislocation walls and kink boundaries, buckling, and delamination. The delaminations are not random, but successively bisect the delaminating sections. The delaminations and associated damage are bound by the kink boundaries. This containment of damage is believed to play a major role in these layered ternary compounds in their damage-tolerant properties.

ACKNOWLEDGMENTS

We thank our colleagues, Professors A. Zavaliangos, S. Kalidindi, and A. Lau, as well as Dr. I. Levin for stimulating discussions. Partial support of Stein Foundation is greatly appreciated by LF. This work was sponsored by the Air Force Office of Scientific Research.

APPENDIX A

The relationship between the radius of curvature (r) that can be provided by arrays of edge dislocations with a Burgers vector $\boldsymbol{b}$, spaced a distance of x apart, within arrays that are spaced a distance of d apart, is[32]

$$r = (x \cdot d)/\mathbf{b} \qquad [A1]$$

From Figure 6, taking, conservatively, $\mathbf{b} \approx 0.3$ nm[29], $d \approx 100$ nm, and $x \approx 20$ nm, one obtains $r \approx 7\ \mu$.

The corresponding angle of rotation (Ω), provided by a bent lamella of length l, is

$$\Omega = l/r$$

Once again from Figure 6, conservatively, the length of the lamella S_2 is $\approx 0.5\ \mu$m. The misorientation angle is ≈ 0.07 rad, or 4 deg. According to SAD (Fig. 6 (b)), the actual angle is closer to 50 deg. Hence, dislocation arrays cannot be a major contributor to lattice rotation in the bent regions observed.

REFERENCES

1. M.W. Barsoum and T. El-Raghy: *J. Am. Ceram. Soc.*, 1996, vol. 79, pp. 1953-56.
2. M.W. Barsoum and T. El-Raghy: *J. Mater. Synth. Proc.*, 1997, vol. 5, pp. 203-22.
3. M.W. Barsoum, T. El-Raghy, and L. Ogbuji: *J. Electrochem. Soc.*, 1997, vol. 144, pp. 2508-16.
4. T. El-Raghy, A. Zavaliangos, M.W. Barsoum, and S. Kalidinidi: *J. Am. Ceram. Soc.*, 1997, vol. 80, pp. 513-16.
5. M.W. Barsoum and T. El-Raghy: *Metall. Mater. Trans. A*, 1999, vol. 30A, pp. 363-69.
6. L. Farber, M.W. Barsoum, A. Zavaliangos, T. El-Raghy, and I. Levin: *J. Am. Ceram. Soc.*, 1998, vol. 81, pp. 1677-81.
7. M.S. Patterson and L.E. Weiss: *Geol. Soc. Am. Bull.*, 1996, vol. 77, pp. 343-73.
8. O. Mugge: *Neues Jarrb. Miner.*, 1898, vol. 1, p. 71.
9. N.C. Gay and L.E. Weiss: *Tectonphysics*, 1974, vol. 21, pp. 287-300.
10. R.E. Robertson, M.G. Sporer, T.Y. Pan, and V.E. Mindroin: *J. Mater. Sci.*, 1989, vol. 24, pp. 4106-13.
11. R.E. Robertson; *J. Polymer Sci.*, 1969, Part A-2, vol. 7, pp. 1315-28.
12. S. DeTeresa, R. Porter, and R. Farris: *J. Mater. Sci.*, 1988, vol. 23, pp. 1886-94.
13. D.A. Zaukelies: *J. Appl. Phys.*, 1962, vol. 33, pp. 2797-2803
14. G.E. Attenburrow and D.C. Bassett: *J. Mater. Sci.*, 1979, vol. 14, pp. 2679-87.
15. A. Keller and J.G. Rider: *J. Mater. Sci.*, 1966, vol. 1, pp. 389-98.
16. C.T. Keith and W.A. Cote, Jr.: *Forest Prod. J.*, 1968, vol. 18, pp. 67-78.
17. H.M. Hathorne and E. Teghtsoonian: *J. Mater. Sci.*, 1975, vol. 10, pp. 41-51.
18. W.R. Jones and J.W. Johnson: *Carbon*, 1971, vol. 9, pp. 645-55.
19. V. Gupta, K. Anand, and M. Kryska: *Acta. Metall. Mater.*, 1994, vol. 42, pp. 781-95.
20. C.W. Weaver and J.G. Williams: *J. Mater. Sci.*, 1975, vol. 10, pp. 1323-33.
21. A.A.S. Argon: *Treatise Mater. Sci. Technol.*, 1972, vol. 1, p. 79.
22. E. Orowan: *Nature*, 1942, vol. 149, pp. 463-64.
23. J.B. Hess and C.S. Barrett: *Trans. AIME*, 1949, vol. 185, pp. 599-606.
24. S. Turan and K.M. Knowles: *Phys. Status Solidi (a)*, 1995, vol. 150, pp. 227-37.
25. H. Suematsu, T. Suzuki, T. Iseki, and T. Mori: *J. Am. Cer. Soc.*, 1991, vol. 74, pp. 173-78.
26. F.C. Frank and A.N. Stroh: *Proc. Phys. Soc. B*, 1952, vol. 65, pp. 811-21.
27. A.N. Stroh: *Proc. R. Soc. London A*, 1954, vol. 223, pp. 404-14.
28. E.G. Tapetado and M.H. Loretto: *Phil. Mag.*, 1974, vol. 30, p. 515.
29. L. Farber, I. Levin, and M.W. Barsoum: *Phil. Mag. Lett.*, 1999, vol. 79, pp. 163-70.
30. T. El-Raghy, M.W. Barsoum, A. Zavaliangos, and S. Kalidindi: unpublished research.
31. I.M. Low, S.K. Lee, B. Lawn, and M.W. Barsoum: *J. Am. Ceram. Soc.*, 1998, vol. 81, 225-28.
32. A.H. Cotrell: *Dislocations and Plastic Flow in Crystals*, Oxford University Press, Cambridge, United Kingdom, 1953.